A Study of the Redox Properties of MoO_x/SiO_2

Nicholas Ohler and Alexis T. Bell*

Department of Chemical Engineering, University of California, Berkeley, California 94720-1462

Received: August 16, 2005

A sample of MoO_x/SiO_2, in which all of the Mo cations are present as isolated mono-oxo molybdate moieties, was prepared and investigated to understand the redox chemistry of such molybdate species and their ability to exchange oxygen with O_2 and H_2O. Raman spectroscopy was used to monitor the exchange of ^{18}O for ^{16}O in the Mo═O bond of isolated molybdate species, whereas mass spectrometry was used to follow the isotopic composition of the gaseous species, i.e., O_2 and H_2O. Reduction in H_2 at 920 K results in the loss of one O atom per Mo atom, and consistent with this, all of the Mo^{VI} cations are reduced to Mo^{IV} cations. Raman spectroscopy shows that virtually all Mo═O bonds of the original molybdate species are lost upon reduction. While reoxidation of Mo^{IV} cations by O_2 is quantitative, studies using $^{18}O_2$ reveal that only a small part of the newly formed Mo═O bonds are ^{18}O labeled, and that the balance are ^{16}O labeled, indicating that O-atom exchange between the support, SiO_2, and the supported MoO_x species occurs during reoxidation. Rapid exchange of O atoms was observed upon exposure of both bare SiO_2 and MoO_x/SiO_2 to $H_2{}^{18}O$ at 920 K, and the presence of MoO_x species was found to enhance the rate of exchange. By contrast, very slow exchange of O atoms was observed when the oxidized catalyst was exposed to $^{18}O_2$ at 920 K. In situ observations of the catalyst during exposure to a mixture of H_2 and $^{18}O_2$ at 920 K showed that all of the Mo cations remained in the VI oxidation state and that O atom exchange occurred at a rate comparable to that observed upon exposure to $H_2{}^{18}O$. The results of this investigation suggest that reoxidation of Mo^{IV} cations following H_2 reduction involves the formation of a Mo−peroxide species and subsequent O atom migration from such a species to the SiO_2 support. It is proposed that the steady-state oxidation of H_2 also involves the formation of Mo−peroxide species by interaction of O_2 with a small number of Mo^{IV} centers. The Mo−peroxide species are then rapidly reduced by H_2 to form H_2O and a Mo═O bond. The rapid exchange of O atoms between the gas phase and the catalyst observed during steady-state oxidation of H_2 is attributed to interactions of the product H_2O with the catalyst, rather than to O atom migration originating from the Mo−peroxide species formed on the catalyst surface.

Introduction

Dispersed molybdena catalysts are active for a variety of reactions, including olefin metathesis,[1] selective oxidation reactions,[2−4] the oxidative dehydrogenation of low-molecular-weight alkanes,[5] the oxidation of NH_3,[6] and the selective catalytic reduction of NO by NH_3.[7] For all of these reactions, the dispersed molybdena species are believed to undergo reduction and oxidation as part of the catalytic cycle. As a result, there is considerable interest in understanding the redox properties of supported MoO_x. The pursuit of this objective is difficult because dispersed molybdena can occur in a variety of forms, i.e., isolated monomolybdate units, polymolybdate domains, or bulk MoO_3 crystallites.[8] Since the reactivity of supported MoO_x catalysts is dependent on the MoO_x structure,[3,9,10] detailed studies of the redox chemistry of dispersed molybdena are best accomplished by limiting the distribution of molybdate species. An attractive means for achieving this is to disperse molybdena on an irreducible support, such as SiO_2. At loadings of less than ∼1 Mo/nm^2, research by a number of groups has shown that it is possible to obtain isolated, monomeric molybdates in this manner.[11−19] After calcination, all of the Mo in these structures is Mo^{VI}. One- or two-electron reduction of isolated molybdates can be achieved using NH_3 or H_2, respectively.[6,20] Oxidation of the resulting Mo^V and Mo^{IV} cations by O_2 leads to full reoxidation of these cations to Mo^{VI}. In the case of reduction by H_2 at 623 K, the stoichiometries of reduction and reoxidation are given by[20]

$$Mo^{VI}O_x + H_2 \rightarrow Mo^{IV}O_{x-1} + H_2O$$

$$2Mo^{IV}O_{x-1} + O_2 \rightarrow 2Mo^{VI}O_x$$

While it is not difficult to envision how H_2 reduction could occur at an isolated MoO_x center, it is much more difficult to understand how two isolated MoO_x centers separated by ∼10 Å or more are reoxidized by O_2. One possibility is that O atom transport occurs on the surface of SiO_2, thereby enabling two Mo^{IV} cations to be oxidized by one molecule of O_2. This hypothesis may explain why a large fraction of the oxygen associated with SiO_2 is incorporated into the products of CH_4 oxidation formed over highly dispersed MoO_x/SiO_2.[21]

The objective of this work was to develop a detailed understanding of the processes involved in the reduction and reoxidation of highly dispersed MoO_x species supported on the surface of SiO_2. Extended X-ray absorbtion fine structure (EXAFS), X-ray absorption near-edge spectroscopy (XANES), and Raman spectroscopy were used to track the structure of

* To whom correspondence may be addressed: bell@cchem.berkeley.edu.

10.1021/jp058230t CCC: $30.25
Published on Web 11/15/2005

MoO_x species and the oxidation state of Mo during sequential reduction by H_2 and reoxidation by O_2, and during steady-state combustion of H_2. Isotopic tracing experiments involving $^{18}O_2$ and $H_2{}^{18}O$ were conducted in order to investigate the exchange of O atoms between oxygen-containing gas-phase species, dispersed MoO_x species, and the SiO_2 support. The experimental results accumulated in the course of this study were then used to propose models for the reduction and oxidation of MoO_x species and to explain the observed exchange of oxygen isotopes between the support and the dispersed MoO_x species.

Experimental Section

Sample Preparation. Silica gel (Silicycle R10070B-00, 60 Å pore diameter) was washed in 9 M HNO_3 at 333 K, rinsed thoroughly with deionized water, and calcined in flowing air for 3 h at 973 K in order to remove alkaline earth impurities.[22,23] This treatment reduced the silica surface area from 500 m^2/g to 460 m^2/g, as measured by five-point analysis of the Brunauer−Emmet−Teller adsorption isotherm. MoO_x/SiO_2 was prepared by aqueous impregnation with ammonium heptamolybdate (AHM) tetrahydrate (Aldrich, 99.98% pure). We suspended 0.067 g of AHM in 2.1 g of deionized water (150% of the pore-filling amount) for each gram of silica gel to be impregnated. The expected Mo loading was 3.5 wt % elemental Mo. The suspension was stirred in a bath heated at 333 K until the solvent was evaporated. The resulting solid was oven-dried at 383 K overnight and calcined under flowing air at 873 K for 3 h. The surface area of the calcined catalyst was 426 m^2/g. The Mo weight fraction determined by elemental analysis (Galbraith Laboratories) was 3.0% (4.5 wt % as MoO_3) so that the nominal surface coverage of MoO_x was 0.44 Mo/nm^2.

Characterization of MoO_x/SiO_2 by X-ray Absorption Spectroscopy. X-ray absorption spectroscopy (XAS) was performed at the Stanford Synchrotron Radiation Laboratory on beamline 2-3 using a Si(220) monochromator. The pre-monochromator slit was reduced to 150 μm to improve energy resolution, and the monochromator was detuned to 90% of the maximum intensity of the rocking curve to remove higher harmonics. Mo K-edge (20 keV) absorption data were collected in transmission mode. MoO_x/SiO_2 (250 mg) was ground into a fine powder and pressed into self-supporting pellets as previously described,[24] resulting in an edge jump $\Delta\mu L$ of ~0.7. MoO_x/SiO_2 samples were pretreated by heating at 10 K/min to 873 K in flowing 10% O_2/He, holding at 873 K for 2 h, and then cooling to room temperature, after which the sample was evacuated to a residual pressure of $\sim 10^{-5}$ Torr. The cell was then repressurized with 10% O_2/He (Matheson certified standard) or H_2 (Praxair UHP), and then the sample was heated under continuous gas flow at 10 K/min to 873 K, at which temperature spectra were recorded. Samples were then cooled to room temperature, then cooled further to 77 K with liquid N_2, and spectra were gathered again.

MoO_3 (Strem, 99.999%), MoO_2 (Strem, 99%), $(NH_4)_6Mo_7O_{24}\cdot 4H_2O$ (Aldrich, 99.98%), $(NH_4)_2Mo_2O_7$ (Strem, 99%), and $Na_2MoO_4\cdot 2H_2O$ (Aldrich, 99.99%) were used as Mo standards. Masses of Mo standards were calculated to target an edge jump $\Delta\mu L$ of 1 using standard photoabsorption cross-section reference data.[25] Mo standards were diluted in BN to make self-supporting pellets of ~70 mg. Standards were evacuated to a residual pressure of $\sim 10^{-5}$ Torr and cooled to 77 K with liquid N_2 prior to the acquisition of XAS data. Total absorption μL was between 1.1 and 1.8 in the post-edge region for all samples. Steps of 10 eV, 0.25 eV, 1 eV, 0.05 $Å^{-1}$, and 0.07 $Å^{-1}$, and collection times of 0.5, 1, 1, 2, and 3 s, were used in the energy regions from −270 to −30 eV, −30 to 30 eV, 30 to 300 eV, 8.9 to 12 $Å^{-1}$, and 12 to 16 $Å^{-1}$, respectively. The spectrum of Mo foil was acquired simultaneously with that of the sample in order to calibrate the Mo K-edge energy. For this purpose, a Mo foil was placed between the detector after the sample (I_1) and a final detector (I_2). Pure Ar was used as the detector gas.

TABLE 1: Edge Energies Relative to Mo Foil.[a]

sample	gas	edge energy (eV)	area of pre-edge peak (eV)
Mo foil	vacuum	0	
MoO_2	vacuum	5.3	
MoO_3	vacuum	6.8	1.8
$(NH_4)_2Mo_2O_7$	vacuum	7.5	2.3
$(NH_4)_6Mo_7O_{24}$	vacuum	7.8	1.6
Na_2MoO_4	vacuum	8.7	3.1
MoO_x/SiO_2	10% O_2/He	8.1	2.2
MoO_x/SiO_2	H_2	5.0	1.0

[a] Spectra of Mo Standards Recorded under Vacuum at 77 K; Spectra of MoO_x/SiO_2 Recorded under Flowing 10% O_2/He or H_2 at 873 K.

EXAFS data were analyzed with the Athena XAS software analysis package.[26] Spectra were gathered in triplicate, aligned using the Mo foil spectra, normalized by fitting cubic splines over the pre-edge region from −150 to −75 eV and over the post-edge region from 0.5 to 16.0 $Å^{-1}$, and averaged. The Autobk method was used to remove background absorption Fourier components of $R < 1.0$ Å, using a k^3-weighted transform ($R_{bkg} = 1.0$ Å) in order to obtain the EXAFS function $\chi(k)$. The k^3-weighted transform of $\chi(k)$ was obtained over the region $2.5 < k < 13.2$ $Å^{-1}$ using a Kaiser−Bessel window.

Characterization of MoO_x/SiO_2 by Raman Spectroscopy. Raman spectra were recorded using a Kaiser Optical HoloLab 5000 series Raman spectrometer equipped with a Nd:YAG laser, frequency-doubled to 532 nm, and operated at 7 mW. The in situ Raman cell employed has been described elsewhere.[27] Samples were ground in a mortar and pestle to a fine powder, pressed at 5 000 psi into self-supporting disks 1 cm in diameter and ~1 mm in depth, and placed on an Au foil located on the rotary stage of the in situ cell. Sample masses were typically 31 mg. He (Praxair UHP), H_2 (Praxair UHP), 10.3% O_2/He (Matheson certified standard), and 20% $^{18}O_2$/He (Isotec, >99% O_2 isotopic purity) were metered into the cell using Porter 201 mass flow controllers. The mass flow controllers were calibrated at multiple points with a soap bubble meter. Flow setpoints were applied manually using a Porter PCIM-4 control unit. $H_2{}^{18}O$ was introduced into the He stream by directing the flow through a 15 mL gas-washing bottle (LabGlass ML-1490-710) filled with $H_2{}^{18}O$ (Isotec/Sigma-Aldrich, >95% O isotopic purity) at room temperature and with 1 mm glass beads (Cole-Parmer 36270-50) to raise the liquid level. All tubing and valves located downstream of the gas washing bottle were maintained at ~333 K to prevent condensation. Total gas flow rates were 20 or 31 cm^3(STP)/min. The heated volume of the Raman cell was estimated to be 15 cm^3. Four-way crossover valves (Swagelok 40 series) were used to switch between gas flows.

Discrete H_2 reduction/$^{18}O_2$ oxidation cycles were monitored in the Raman cell using the pulse apparatus described below for reducing MoO_x/SiO_2 in a continuous H_2 flow and reoxidizing with pulses of $^{18}O_2$ at 920 K. The temperature of the Raman cell was controlled with an Omega CN8500 controller using feedback from a type-K thermocouple located in a quartz thermocouple well positioned 1 cm above the sample. The temperature at the sample surface was measured without the

cell rotating, and was found to be 920 K with the control thermocouple at 873 K. The sample was rotated at ~150 rpm in order to distribute the laser beam over a large area, thereby preventing the overheating of the sample. Under static conditions, three 90 s exposures were averaged in order to obtain spectra with a high signal-to-noise ratio. During transient-response experiments, each spectrum was recorded using a single 30 s exposure in order to improve temporal resolution. In all cases, cosmic rays were filtered using automated algorithms within the HoloLab control software by performing each exposure twice. Spectra were gathered in the Stokes-scattering region from the Rayleigh-scattering filter cutoff of ~150 cm^{-1} up to 4460 cm^{-1}.

Background fluorescence was removed from Raman spectra by fitting a quadratic function

$$a + b(\nu - \nu_0)^2$$

with adjustable parameters a, b, and ν_0 to the region from ν = 1350 to 2000 cm^{-1} in which no peaks appear, excluding the region from 1540 to 1580 cm^{-1} where a peak for O_2 appears. The residual spectra were fit over the range from 330 to 1300 cm^{-1} with Lorentzian line shapes

$$\frac{A_i}{2\pi}\frac{\Gamma_i}{(\nu - \mu_i)^2 + \left(\frac{\Gamma_i}{2}\right)^2}$$

where i is the peak index, A_i is the peak area (counts × s^{-1} × cm), Γ_i is the full width at half-maximum (cm^{-1}), and μ_i is the position of the peak maximum (cm^{-1}).

The Raman features of SiO_2 are well known.[28−32] The spectra of bare SiO_2 were fit by including a Lorentzian component for each of the Raman-active SiO_2 features including the network features ω_1 (450 cm^{-1}), ω_3 (800 cm^{-1}), ω_4 (TO) (1065 cm^{-1}), and ω_4 (LO) (1200 cm^{-1}); the defect features D_1 (495 cm^{-1}) and D_2 (606 cm^{-1}); and the Si−OH stretch (970 cm^{-1}). Observed peak positions μ_i of the well-resolved ω_3 and D_2 features were ~8 cm^{-1} higher than those previously reported for $Si^{16}O_2$,[28] possibly due to differences in calibration and/or differences in SiO_2 sample morphology. The parameters A_i, Γ_i, and μ_i were varied for each feature in order to fit the spectrum of SiO_2.

The spectra of MoO_x/SiO_2 were fit by including Lorentzian components for the known Mo═O stretching vibration (986 cm^{-1}) and Mo═O bending vibration (310 cm^{-1}).[9,13] The Mo═O stretching band of $^{16}O_2$-calcined MoO_x/SiO_2 was observed at 988 cm^{-1}. A Lorentzian component was also included at 925 cm^{-1} to account for a feature appearing as a shoulder on the Mo═O stretch. A feature at 925 cm^{-1} has previously been reported in the IR spectrum of MoO_x/SiO_2 and assigned to vibrations of Mo−O−Si bonds.[33,34] During ^{18}O exchange the Mo═^{16}O band at 988 cm^{-1} decreased in intensity and a separate Mo═^{18}O band appeared at 938 cm^{-1}, which increased in intensity. The observed −50 cm^{-1} shift in band position upon substitution of ^{18}O by ^{16}O in Mo═O is consistent with the −49 cm^{-1} shift observed previously by IR spectroscopy for MoO_x/SiO_2 after room-temperature exchange with $H_2{}^{18}O$.[35] A separate Lorentzian component was added at 938 cm^{-1} to fit spectra including this peak. The fraction of the molybdenyl occupied by ^{16}O was calculated from the fraction of the total Mo═O area in the 938 cm^{-1} peak:

$$\frac{A_{938}}{A_{938} + A_{988}}$$

Due to the overlap of the Mo−O−Si, Si−OH, ω_4(TO), ω_4-(LO), and Mo═O isotopomer features in the region of 900−1200 cm^{-1}, the Lorentzian parameters of all of the peaks could not be determined uniquely by fitting the spectrum of MoO_x/SiO_2. The Lorentzian parameters of the Si−OH, ω_4(TO), and ω_4(LO) features were thus correlated to the position of the well-resolved D_2 peak using data gathered during O exchange over bare SiO_2. The SiOH peak intensity was decreased by 44% to account for the approximate fraction of SiOH sites replaced by MoO_x in the 0.44 Mo/nm^2 MoO_x/SiO_2. Since the Mo−O−Si feature overlapped with the Mo═O feature and was small, it was not possible to monitor the red shift of the Mo−O−Si feature by allowing the Mo−O−Si peak position to vary as ^{18}O was exchanged into the surface. However, because the Mo−O−Si peak was small and broad, its position and width were simply held constant in order to fit the spectra of MoO_x/SiO_2 as ^{18}O was exchanged into the surface. The fitting procedure resulted in a total peak area for the two Mo═O isotopomer bands that was constant to within ±5 relative %, allowing reliable observation of the isotopic composition of the Mo═O bonds.

Because the ω_1 and D_1 features of SiO_2 and the bending feature of Mo═O overlap strongly in the 300−600 cm^{-1} region, the data fitting was unreliable in this region, and the amplitudes and widths of the peaks found from least-squares regression varied widely. However, the positions of the ω_3 and D_2 peaks could be determined with good certainty because they were well-resolved from other spectral features, and the scatter in these peak positions was only ±3 cm^{-1} and ±2 cm^{-1}, respectively, during collection of spectra under dynamic conditions (single 30 s exposures). Red shifts for these features upon replacement of ^{16}O with ^{18}O have been reported as 12 and 31 cm^{-1}, respectively.[28] Hence the scatter in the ω_3 peak position was too large, relative to its red shift, to use it reliably as a measure of ^{18}O incorporation into SiO_2, but the D_2 peak could be used as such a metric. The D_2 feature arises from features at the SiO_2 surface, attributed to either cyclic $(Si-O-)_3$ moieties[28,29] or homopolar Si−Si and O−O bonds.[31,32] It was assumed that the D_2 peak position is linearly proportional to the fraction of oxygen incorporated in the feature that was 18-labeled, so the fraction of ^{16}O in the feature was calculated as the accomplished change in the peak position:

$$\frac{\mu_{D_2} - \mu_{D_2}{}^{18}}{\mu_{D_2}{}^{16} - \mu_{D_2}{}^{18}}$$

μ_{D_2} is the peak position of the D_2 feature, and $\mu_{D_2}{}^{16}$ and $\mu_{D_2}{}^{18}$ are the peak positions of the D_2 feature with pure ^{16}O and pure ^{18}O, respectively. The $^{16}O \rightarrow {}^{18}O$ red shift of the D_2 feature $\mu_{D_2}{}^{16} - \mu_{D_2}{}^{18}$ was taken as 33 cm^{-1}. Scatter was substantially less when spectra were gathered under static conditions (three 90 s exposures averaged), and the standard deviation of the D_2 peak position of eight such spectra taken under static conditions was 0.34 cm^{-1}.

Reduction and Oxidation of MoO_x/SiO_2. O_2 pulse chemisorption was performed at 873 K on H_2-reduced MoO_x/SiO_2 according to established procedures.[20] The TCD detector of an Agilent 6890N gas chromatograph was used to detect O_2 not adsorbed by the samples. Data points were gathered at a frequency of 5 Hz. Calcined samples of ~100 mg were loaded

into a quartz microreactor (described elsewhere),[36] heated at 10 K/min to 873 K and held for 30 min, purged in pure He for 15 min, reduced in pure H_2 for 30 min, and purged in He until the detector signal reached the baseline (~20 min). Four-way switching valves (Swagelok 40 series) were used to switch between gas flows. All gas flow rates were maintained at 30 cm^3(STP)/min. Square pulses containing 1.79 μmol of O_2 were introduced at room temperature into the He stream using a six-way crossover valve (Swagelok 40 series). A 0.421 cm^3 sample loop was used to set the pulse size. The loop was filled by flowing 10.3% O_2/He (Matheson certified standard) through it. Pulses were injected into the He stream at 2 min intervals until the detected area was constant for at least three consecutive pulses. The oxygen uptake was calculated from the following equation:

$$n_{\mathrm{O}}^{\mathrm{sample}} = 2n_{\mathrm{O}_2}^{\mathrm{loop}}\left(\frac{NA_{\mathrm{f}} - \sum_{i=1}^{N} A_i}{A_{\mathrm{f}}}\right)$$

where $n_{\mathrm{O}}^{\mathrm{sample}}$ is the moles of O adsorbed by the sample, $n_{\mathrm{O}_2}^{\mathrm{loop}}$ is the moles of O_2 contained in a full pulse, N is the total number of pulses injected, A_i is the detected area of the i-th pulse, and A_{f} is the area of the final pulse, corresponding to a full pulse. Chemisorption of O_2 by the H_2-reduced empty reactor was small but measurable (~0.5 μmol of O), and this amount was subtracted from the amount adsorbed by H_2-reduced MoO_x/SiO_2 samples, which was on the order of 36 μmol of O. O_2 chemisorption by H_2-reduced bare SiO_2 was also tested, but no measurable adsorption was observed.

Analysis of Gas-Phase Composition during Isotope Exchange Experiments. Isotopic exchange experiments were carried out to determine the rates at which gas-phase $^{18}O_2$ and $H_2{}^{18}O$ exchange O atoms with the catalyst. These experiments were carried out in the Raman cell. The isotopic composition of the effluent from the Raman cell was monitored with an MKS Minilab mass spectrometer. Data were gathered in analog mode with 16 points per mass, sweeping from $m/e = 1-50$. An accuracy setting of 5 was used (2^5 samples per data point), allowing the collection of one mass spectrum every 41 s. Peak maxima were used for quantification of partial pressures. Response factors were determined relative to He for H_2, O_2, and H_2O by multi-point calibration, and the appropriate corrections were made to the fragmentation patterns of O_2 and H_2O to account for the natural abundance of ^{18}O. It was assumed that the response factors for ^{18}O-containing fragments were identical to those of the corresponding ^{16}O-containing fragments. The O fragment from H_2O was negligibly small in intensity, so $H_2{}^{16}O$ and $H_2{}^{18}O$ could be monitored independently using masses 18 and 20, respectively. H_2, $^{16}O_2$, $^{16}O^{18}O$, and $^{18}O_2$ were monitored independently using masses 2, 32, 34, and 36, respectively. The isotopic composition of the H_2O resulting from H_2-reduction of MoO_x/SiO_2 was calculated by integrating the molar flow rates of H_2O isotopomers over the duration of the reduction and comparing their integral amounts.

Results and Discussion

Structural Characterization. The structure of the MoO_x species dispersed on the surface of SiO_2 sample was investigated by X-ray absorption spectroscopy (EXAFS and XANES). The magnitude of the Fourier transformed, k^3-weighted EXAFS data ($k^3\chi(k)$) for MoO_x/SiO_2 calcined at 873 K is shown in Figure 1 together with similar data for the Mo standards. Backscattering

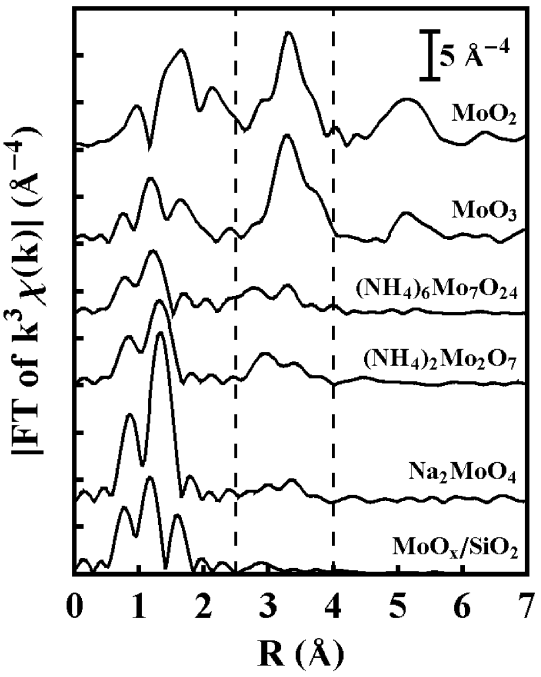

Figure 1. Magnitude of Fourier transform of $k^3\chi(k)$ for calcined MoO_x/SiO_2 and Mo-containing standards, uncorrected for phase shift. Dashed lines identify the Mo−Mo scattering region for Mo−O−Mo moieties. All spectra gathered at 77 K under vacuum.

by Mo atoms is evident between 2.5 and 4.0 Å for MoO_2, MoO_3, $(NH)_4Mo_7O_{24}$, and $(NH_4)_2Mo_2O_7$, all of which contain Mo−O−Mo bonds. Only weak scattering by Na is observed in this region for Na_2MoO_4, and no backscattering is observed in this region for MoO_x/SiO_2. The lack of a backscattering peak between 2.5 and 4.0 Å for MoO_x/SiO_2 has been observed previously, and is indicative of the isolation of MoO_x species from one another.[13,14] This conclusion is consistent with previous studies, which have shown that both polyoxometalates, such as $(NH_4)_6Mo_7O_{24}$ (the precursor used in this work) and molecular precursors containing only a single Mo atom, such as $MoCl_5$ and Mo(η^3-C_3H_5)$_4$, produce identical MoO_x structures upon calcination.[8,15,37] For Mo loadings of less than ~1 Mo/nm^2, only isolated MoO_x species are observed. Site isolation is achieved when the surface concentration of Mo is less than that of the Si−OH groups on the surface of SiO_2, since the Mo precursor reacts directly with Si−OH groups in the initial stages of catalyst preparation.[11,12] Since a surface concentration of ~1 Si−OH/nm^2 is attained upon calcination of SiO_2 at 873 K[38] and since the Mo loading of the catalyst used in this study is 0.44 Mo/nm^2, it was expected that the catalyst used in the present work would contain isolated MoO_x species.

Previous attempts to determine oxygen coordination numbers and Mo−O bond distances from an analysis of EXAFS data have yielded conflicting results.[13,14] The differing conclusions are due to uncertainty in the amount of static disorder in the O shells, and the presence of overlapping atomic absorption peaks in the region of low R values. Conclusions regarding coordination geometry based on UV−visible spectroscopy have also differed due to the broad nature of the UV−visible absorption bands of MoO_x/SiO_2 and the variety of factors influencing UV−visible absorption bands.[8,14,20,39] More useful information concerning the coordination of MoO_x species in samples of MoO_x/SiO_2 has been established by XANES.[13,14,16] The Mo K-edge XANES spectrum of MoO_x/SiO_2 and those of several Mo standards are presented in Figure 2. Spectra of standards were collected at 77 K under vacuum, and that of MoO_x/SiO_2 was

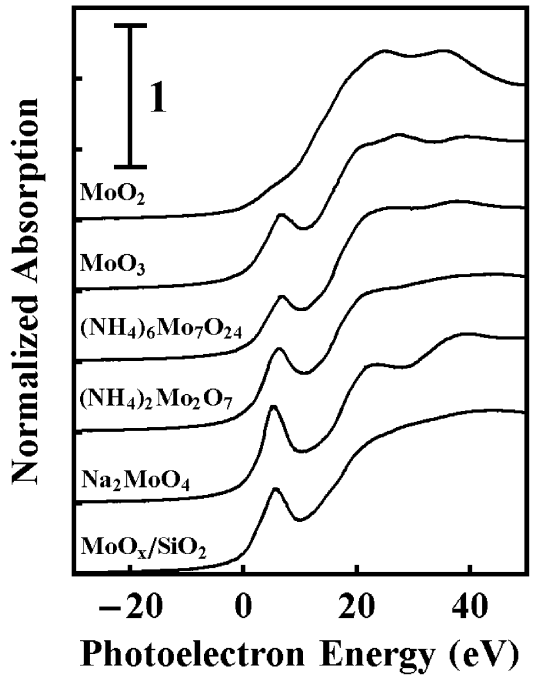

Figure 2. Normalized XANES spectra of MoO_x/SiO_2 acquired at 873 K in flowing 10% O_2/He and of Mo-containing standards acquired at 77 K under vacuum.

collected at 873 K under flowing 10% O_2/He. The pre-edge feature at ~20 005 eV is indicative of transitions from the Mo K-shell to unoccupied valence orbitals, and is larger for less centrosymmetric geometries, for which unoccupied valence orbitals have some p-character.[40,41] The area of the pre-edge feature was determined by integration as in a previous study[14] and increases in the series

$$MoO_2 < (NH_4)_6Mo_7O_{24} \approx MoO_3 < MoO_x/SiO_2 \approx (NH_4)_2MoO_7 < Na_2MoO_4$$

MoO_2 has no pre-edge feature because it is composed of nearly perfect Mo octahedra,[42] which exhibit no p−d mixing and no p-character in the valence shells. $(NH_4)_6Mo_7O_{24}$ and MoO_3 are composed of Mo octahedra that are distorted to different degrees, resulting in some amount of p−d mixing and a small XANES pre-edge feature.[43,44] The pre-edge feature of MoO_x/SiO_2 is approximately equivalent to that of $(NH_4)_2Mo_2O_7$, which is composed of octahedral Mo and tetrahedral Mo in a 1:1 ratio.[45] Na_2MoO_4 contains tetrahedrally coordinated Mo, and the acentric coordination results in the largest pre-edge feature.[46] The relative size of the pre-edge feature of MoO_x/SiO_2 is consistent with previous observations, and is indicative of coordination intermediate between tetrahedral and octahedral.[13,14] The same conclusion has been found based on Mo L-edge XANES.[16] The XANES data, therefore, support previous assignments of dehydrated MoO_x/SiO_2 at low loadings as pentacoordinate.[9,35]

Figure 3 shows the Raman spectra of bare SiO_2 and MoO_x/SiO_2 at 920 K under flowing air. The known Raman features of SiO_2[28] and of MoO_x[8,9,13] are identified, and the shoulder at 925 cm^{-1} is tentatively assigned to a Mo−O−Si vibration.[33,34] The position of the Mo═O stretching band (988 cm^{-1}) and the lack of the intense bands of bulk MoO_3 at 825 and 1001 cm^{-1} (the Mo−O−Mo asymmetric stretch and Mo═O stretch, respectively) indicate that the MoO_x is completely dispersed as isolated MoO_x with a single terminal oxo group,[8,9,47] consistent

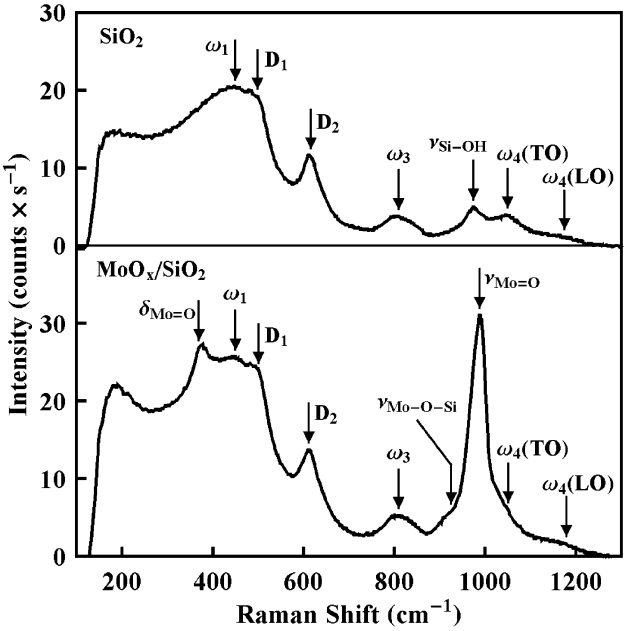

Figure 3. Raman spectra of bare SiO_2 and of MoO_x/SiO_2 acquired at 920 K in flowing air. Raman bands are identified for SiO_2 (ω_1, ω_3, ω_4(TO), ω_4(LO), D_1, D_2, and ν_{Si-OH}) and MoO_x ($\delta_{Mo=O}$, $\nu_{Mo-O-Si}$, and $\nu_{Mo=O}$) supported on SiO_2.

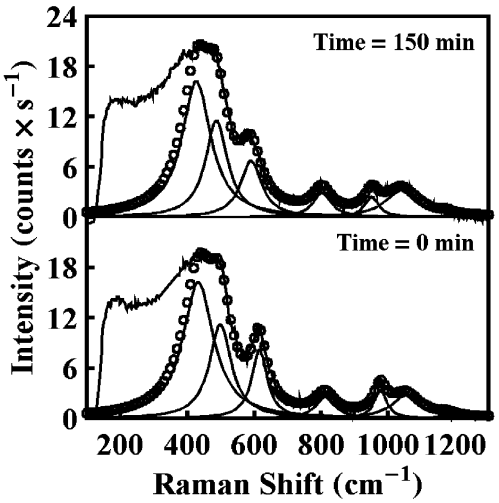

Figure 4. Baseline-subtracted Raman spectrum of bare SiO_2 acquired at 920 K before $H_2{}^{18}O$ exposure and after 150 min of exposure to 3.7% $H_2{}^{18}O$/He. The open circles show the sum of the Lorentzian components used to deconvolute the spectrum. Total gas flow rate was 31 cm^3-(STP)/min; catalyst mass was 31.3 mg.

with the findings above based on X-ray absorption spectroscopy. The combined characterization methods of XAS and Raman spectroscopy demonstrate that the calcined MoO_x/SiO_2 used in this study contains isolated, mono-oxo MoO_x moieties of pentacoordinate geometry.

Isotopic Exchange of O Atoms upon Exposure of MoO_x/SiO_2 to $H_2{}^{18}O$. Figure 4 shows the Raman spectrum of bare SiO_2 calcined in $^{16}O_2$ at 920 K before and after 150 min of exposure to 3.7% $H_2{}^{18}O$/He. After exposure to $H_2{}^{18}O$ at 920 K, red shifts are observed throughout the SiO_2 Raman spectrum. The parameters of the Lorentzian peaks used to fit the SiO_2 D_2 band and the Mo═O isotopomer bands are summarized in Table 2 at various times on stream during the exchange of $H_2{}^{18}O$ with $^{16}O_2$-calcined SiO_2 and MoO_x/SiO_2. After 150 min on stream, the position of the D_2 feature shifted from 614 to 590 cm^{-1}.

TABLE 2: Lorentzian Parameters of SiO_2 D_2 Feature and Mo═O Isotopomer Features at Various Times during Exchange of 3.7% $H_2{}^{18}O$/He with $^{16}O_2$-calcined SiO_2 and during Exchange of 3.3% $H_2{}^{18}O$/He with Air-Calcined MoO_x/SiO_2

		SiO_2 D_2			Mo═^{18}O			Mo═^{16}O		
sample	time on stream (min)	A (counts × s^{-1})	μ (cm^{-1})	Γ (cm^{-1})	A (counts × s^{-1})	μ (cm^{-1})	Γ (cm^{-1})	A (counts × s^{-1})	μ (cm^{-1})	Γ (cm^{-1})
bare SiO_2	0	727	614	58						
	8	730	610	63						
	150	687	590	68						
MoO_x/SiO_2	0	719	614	48				1530	988	38
	8	668	608	55	697	938	35	746	988	37
	152	499	583	53	1280	938	32	140	988	35

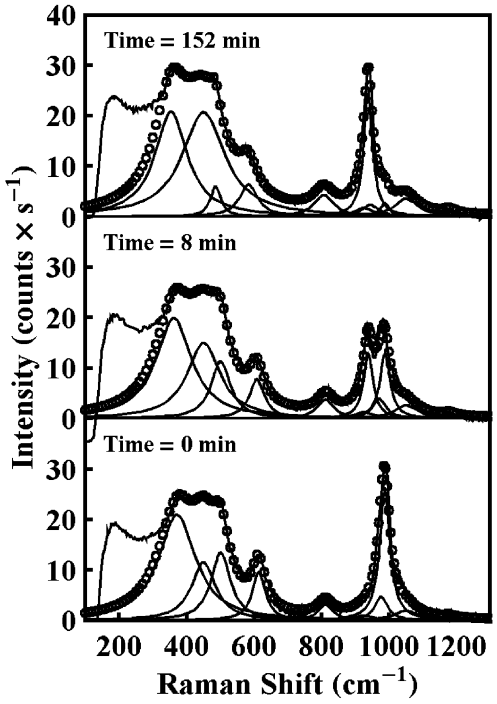

Figure 5. Baseline-subtracted Raman spectrum of MoO_x/SiO_2 acquired at 920 K before $H_2{}^{18}O$ exposure and after 8 and 150 min under 3.3% $H_2{}^{18}O$/He. The open circles represent the sum of the Lorentzian components used to deconvolute the spectrum. Total gas flow rate was 31 cm^3(STP)/min; catalyst mass was 31.5 mg.

Based on the accomplished change in the D_2 peak position, 73% of the SiO_2 surface oxygen was exchanged with the gas phase at this time. Direct exchange of oxygen with the SiO_2 surface can occur by dissociative adsorption of $H_2{}^{18}O$ to cleave siloxane bonds, followed by dehydration of the surface to release $H_2{}^{16}O$:

$$\mathrm{Si{-}{}^{16}O{-}Si + H_2{}^{18}O \rightleftarrows Si{-}{}^{16}OH + Si{-}{}^{18}OH \rightleftarrows Si{-}{}^{18}O{-}Si + H_2{}^{16}O}$$

Figure 5 shows the Raman spectrum of MoO_x/SiO_2 at 920 K calcined in air and after 8 and 152 min of exposure to 3.3% $H_2{}^{18}O$/He. The oxygen of the Mo═O group exchanges rapidly with that of gaseous H_2O, suggesting that hydrolysis and dehydration occur readily for the doubly bonded oxygen of MoO_x:

$$\mathrm{Mo{=}{}^{16}O + H_2{}^{18}O \rightleftarrows HO^{18}{-}Mo{-}{}^{16}OH \rightleftarrows Mo{=}{}^{18}O + H_2{}^{16}O}$$

After 8 min on stream, the intensity of the Mo═^{16}O stretching band at 988 cm^{-1} decreased by about half, and the band for Mo═^{18}O at 938 cm^{-1} rose to about equivalent intensity. After 152 min on stream, about 90% of the Mo═^{16}O was replaced by Mo═^{18}O, and the D_2 peak position shifted from 614 to 583 cm^{-1}. Based on the D_2 peak position, 93% of the SiO_2 surface oxygen was exchanged with the gas phase after 152 min.

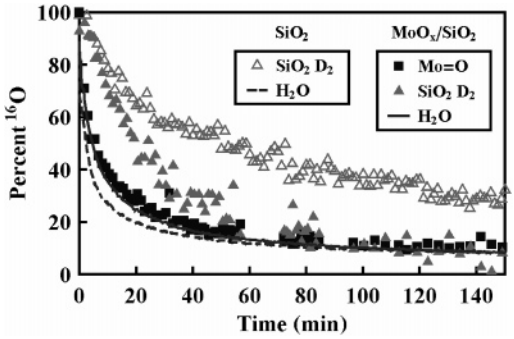

Figure 6. Isotopic compositions of the D_2 feature of SiO_2 and gaseous H_2O during oxygen exchange at 920 K between $^{16}O_2$-calcined SiO_2 and 3.7% $H_2{}^{18}O$/He and isotopic compositions of the Mo═O, the D_2 feature of SiO_2, and gaseous H_2O during oxygen exchange at 920 K between $^{16}O_2$-calcined MoO_x/SiO_2 and 3.3% $H_2{}^{18}O$/He. Total gas flow rate was 31 cm^3(STP)/min; catalyst masses were 31.3 mg of SiO_2 and 31.5 mg of MoO_x/SiO_2, respectively.

Figure 6 shows the isotopic compositions of the water vapor effluent from the reactor as a function of time when air-calcined SiO_2 or MoO_x/SiO_2 was contacted with $H_2{}^{18}O$ at 920 K. The isotopic composition of the D_2 feature of SiO_2 is shown for both samples, and the Mo═O isotopic composition is shown for MoO_x/SiO_2. During oxygen exchange between $H_2{}^{18}O$ and bare SiO_2, the isotopic composition of the H_2O falls to <20% $H_2{}^{16}O$ in 20 min, then decreases slowly to 8% $H_2{}^{16}O$ after 150 min. The isotopic composition of the D_2 feature of SiO_2 decreases to 60% ^{16}O in 25 min, then decreases at a slower rate to 29% after 150 min. Exchange of oxygen between H_2O and the D_2 feature of SiO_2 is limited kinetically, as the fraction of ^{16}O in the D_2 band is greater than that in H_2O at any time during the exchange. By contrast, the exchange of oxygen between H_2O and the Mo═O group of MoO_x/SiO_2 is rapid, and is essentially equilibrated; the Mo═O isotopic composition is equivalent to that of H_2O throughout the exchange with MoO_x/SiO_2. Hence, the isotopic composition of Mo═O is a good indicator of the isotopic composition of H_2O. This point will be of use in the analysis of the trends in isotopic composition during H_2 oxidation by $^{18}O_2$ discussed below.

The H_2O isotopic composition is more ^{16}O-rich for times on stream of less than 80 min during exchange with MoO_x/SiO_2 than it is during exchange with SiO_2, and it approaches the same asymptote at longer times on stream, approaching 8% ^{16}O at 150 min. This suggests the presence of rapidly exchanging surface oxygen on MoO_x/SiO_2, which enriches the $H_2{}^{16}O$ isotopic composition at short times on stream, but not at longer

TABLE 3: Rate Constants and Pool Sizes of Surface Oxygen Pools Exchanging with Gaseous H_2O

	k (atm × min)$^{-1}$	n
SiO_2	6.0	0.20 O/Si[a]
	0.35	0.72 O/Si[a]
MoO_x	≥100	1 O/Mo
	6.0	8.5 O/Mo

[a] Conversion factor: in MoO_x/SiO_2 with 3.0 wt % Mo, there are 51 Si/Mo.

times on stream when the rapidly exchanging surface oxygen has equilibrated in isotopic composition with that of gaseous H_2O. The ^{16}O fraction of the oxygen of the D_2 feature of SiO_2 decreases at a slightly higher initial rate during exchange between H_2O and MoO_x/SiO_2 than it does during exchange between H_2O and SiO_2. The oxygen of the D_2 feature of SiO_2 also exchanges to a greater extent during exchange between H_2O and MoO_x/SiO_2 than it does during exchange between H_2O and SiO_2, approaching the isotopic composition of the gas phase in ~100 min.

The amount of surface oxygen (^{16}O) exchanged into the gas phase over the course of the experiment was determined by fitting of gas-phase data to a kinetic model, assuming complete backmixing of the gas phase within the reactor. Such a procedure was necessary to quantify the amount of exchangeable surface oxygen because of the large amount of slowly exchanging surface oxygen associated with the surfaces of the Raman cell. The details of the kinetic model are presented in the Supporting Information. The rate constants and sizes of the oxygen pools determined by the procedure are presented in Table 3. Two oxygen pools were required in order to describe the exchangeable surface oxygen of SiO_2, one exchanging with a moderate rate constant of 6.0 (atm min)$^{-1}$ and a size of 0.20 O per Si, the other with a lower rate constant of 0.35 (atm min)$^{-1}$ and a size of 0.72 O per Si (the total oxygen inventory of bare SiO_2 is 2 O per Si). Based on the surface area of the SiO_2 used in this study (460 m^2/g), it is estimated that surface oxygen accounts for 22% of the total oxygen inventory of bare SiO_2, or 0.44 O per Si. Based on the sizes of the oxygen pools observed, 45% of the surface oxygen of SiO_2 exchanges with gaseous H_2O at a moderate rate, and an additional 164% of the surface oxygen exchanges slowly. The slow-exchanging oxygen pool of SiO_2 accounts for about a third of the total oxygen inventory of SiO_2, and probably represents diffusion of the bulk oxygen of SiO_2 to the surface followed by gas−surface oxygen exchange.

To fit the gas-phase data collected over MoO_x/SiO_2, one oxygen per Mo was included with a very large rate constant of 100 (atm min)$^{-1}$ to account for the Mo=O oxygen, observed by Raman spectroscopy to rapidly equilibrate with the oxygen of gaseous H_2O. The second oxygen pool had the same rate constant, 6.0 (atm min)$^{-1}$, as the moderately exchanging oxygen pool of bare SiO_2, and a pool size of 8.5 O per Mo. Since the rate constant for oxygen exchange was the same for this oxygen pool as for one of the oxygen pools of SiO_2, this suggests that the presence of MoO_x simply allowed more extensive access to the oxygen pool of the SiO_2. This is consistent with the observation made by Raman spectroscopy that exchange of the SiO_2 D_2 feature is more extensive for MoO_x/SiO_2 than for SiO_2. The combined oxygen pools exchanging at 6.0 (atm min)$^{-1}$ account for 18.7 O per Mo exchanging with the gas phase, or 18% of the total oxygen of the catalyst. This is close to the estimate of the total amount of surface oxygen of MoO_x/SiO_2 (21% of the total oxygen inventory), so it appears that all of the surface oxygen of MoO_x/SiO_2 exchanges at a moderate rate with gaseous H_2O, whereas only about half of the surface oxygen of bare SiO_2 exchanges at the same rate. This finding supports the notion that MoO_x moieties supported on SiO_2 act as "portholes",[21] increasing the rate of exchange and extent of exchange of oxygen between H_2O and SiO_2. The manner in which MoO_x facilitates the exchange of O atoms between H_2O and SiO_2 is not well understood. Conceivably, it may be related to stabilization of H_2O adsorbed on SiO_2 caused by hydrogen bonding with the acidic protons of hydrolyzed Mo−O−Si bonds. This could result in an increased surface concentration of physisorbed H_2O on the SiO_2 surface, and hence enhanced oxygen exchange between SiO_2 and H_2O.

Sequential H_2 Reduction and $^{18}O_2$ Reoxidation of MoO_x/SiO_2. The extent to which the Mo^{VI} cations in MoO_x/SiO_2 are reduced upon reaction with H_2 at 873 K was determined by measuring the uptake of O_2 upon reoxidation. Titrations were carried out by pulse chemisorption of O_2 following procedures described elsewhere.[20] H_2 reduction was completely reversible as multiple H_2 reductions and O_2 titrations yielded identical results. O uptake was 1.16 ± 0.02 O per Mo with the moles of Mo calculated based on the results of elemental analysis, or 0.99 ± 0.02 O per Mo with the moles of Mo calculated based on the amount of Mo loaded during catalyst synthesis. This result is consistent with previous titration measurements reported for fully dispersed MoO_x/SiO_2 [20] and with H_2 TPR data for MoO_x/SiO_2, in which peaks accounting for ~1 O per Mo were observed at $T < 879$ K.[48] Therefore, it appears that the sample of MoO_x/SiO_2 utilized in this study was completely dispersed, and that stoichiometric reduction of MoO_x/SiO_2 by H_2 and reoxidation by O_2 at 873 K can be described by

$$Mo^{VI}O_x + H_2 \rightarrow Mo^{IV}O_{x-1} + H_2O$$

$$2Mo^{IV}O_{x-1} + O_2 \rightarrow 2Mo^{VI}O_x$$

The reduction of $Mo^{VI}O_x$ to $Mo^{IV}O_{x-1}$ by H_2 is further supported by XANES. Edge energies were determined for each of the samples relative to Mo foil by aligning the rising slopes of the spectra in the 20 010−20 020 eV range with that of Mo foil. The relative edge energies are tabulated in Table 1. The relative edge energies of the Mo^{VI} standards MoO_3, $(NH_4)_6Mo_7O_{24}$, $(NH_4)_2Mo_2O_7$, and Na_2MoO_4 fall within the 6.8−8.7 eV range, whereas the relative edge energy of the Mo^{IV} standard MoO_2 was 5.3 eV. Figure 7 shows the XANES spectra of MoO_x/SiO_2 at 873 K in flowing air and in flowing H_2, as well as the XANES spectrum of MoO_2 for comparison. In 10% O_2/He, the edge energy of MoO_x/SiO_2 was 8.1 eV, well within the range of energies observed for the various Mo^{VI} standards, whereas in H_2, the edge energy was 5.0 eV, which is very close to that observed for MoO_2. Under flowing H_2, the size of the pre-edge feature of MoO_x/SiO_2 decreases. This results from increased occupation of the valence shell orbitals in the reduced Mo, which decreases the number of available final states for the transitions giving rise to the pre-edge feature.

The reoxidation mechanism of H_2-reduced MoO_x/SiO_2 by O_2 was investigated by performing H_2-reduction/$^{18}O_2$-oxidation cycles. The incorporation of ^{18}O into the sample during reoxidation was monitored by Raman spectroscopy and the isotopic composition of the H_2O produced during reduction was monitored by mass spectrometry. The Raman spectrum of H_2-reduced MoO_x/SiO_2 is shown together with that of $^{16}O_2$-calcined MoO_x/SiO_2 in Figure 8. The spectrum was identical under both flowing H_2 and He following H_2 reduction. Upon reduction,

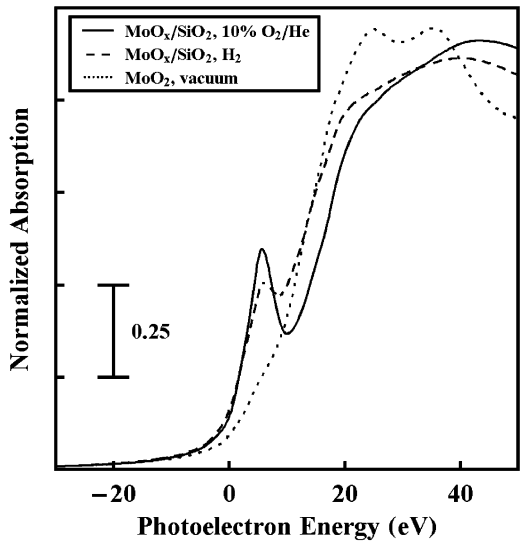

Figure 7. XANES spectra of MoO_x/SiO_2 acquired at 873 K in flowing 10% O_2/He and in flowing H_2 and XANES spectrum of $Mo^{IV}O_2$ acquired at 77 K under vacuum.

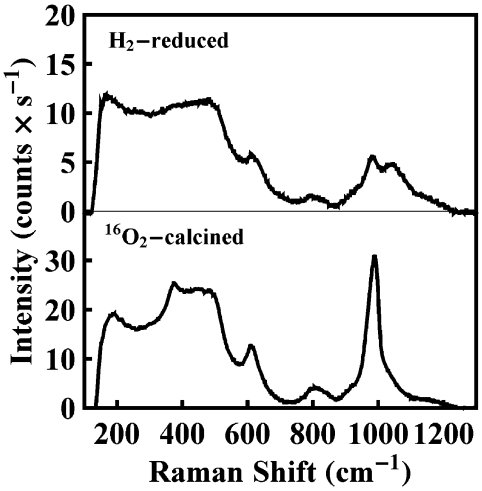

Figure 8. Baseline-subtracted Raman spectrum of MoO_x/SiO_2 acquired at 920 K in flowing 6% $^{16}O_2$/He and in flowing H_2.

the sample takes on a deep blue color and all of the Raman bands are attenuated. The reduction in Raman signal strength is due to lower penetration depth of the laser radiation, due to the higher optical absorbance of the reduced sample. The intense Mo═O stretching feature at 988 cm^{-1} appears to be completely attenuated upon reduction of the sample, as is the Mo═O bending mode at 370 cm^{-1}. All of the SiO_2 peaks remain present in the spectrum of H_2-reduced MoO_x/SiO_2, but the Si−OH stretching feature at 975 cm^{-1} and the SiO_2 ω_4(TO) phonon mode at 1051 cm^{-1} are ∼30% more intense with respect to the SiO_2 D_2 feature at 614 cm^{-1} in the H_2-reduced spectrum of MoO_x/SiO_2 than they are in the spectrum of bare SiO_2. This enhancement may result from increased optical absorption at higher frequencies[49] (the optical frequency of the scattered light decreases with increased vibrational frequency for Stokes scattering). It is also possible that some reduced MoO_x is present as Mo^{IV}═O. However, when a Lorentzian component was added at 988 cm^{-1} to fit the spectrum, the intensity of the component relative to the intensity of the SiO_2 D_2 feature was only 8% of the relative intensity of the Mo═O band prior to H_2 reduction. This represents an upper limit of the fraction of the H_2-reduced MoO_x that has a single terminal oxo ligand. Most or all (≥92%)

SCHEME 1: Interchange between Forms of Mo^{IV} with Zero and One Terminal Oxo Ligands

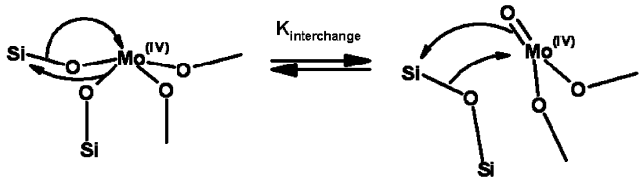

of the H_2-reduced MoO_x is present without a terminal oxo ligand. Since the structure of fully oxidized MoO_x is pentacoordinate with a single terminal oxo ligand, the structure of H_2-reduced MoO_x may be represented by the four-coordinate and three-coordinate forms shown in Scheme 1. It is evident from the observed intensity of the Mo═O band of H_2-reduced MoO_x/SiO_2 that the equilibrium for this interchange lies heavily to the left side ($K_{interchange} \leq 0.09$).

The isotopic composition of the Mo═O oxygen and the oxygen of the SiO_2 D_2 feature are shown in Figure 9 as functions of the number of H_2 reduction/$^{18}O_2$ reoxidation cycles performed. The isotopic composition of the H_2O resulting from H_2 reduction of the catalyst at each step is also shown. As cycles of H_2 reduction and $^{18}O_2$ reoxidation were performed, ^{16}O was depleted from the catalyst and replaced with ^{18}O. However, the large majority of the oxygen replenishing the Mo═O of H_2-reduced MoO_x was ^{16}O from the surface rather than ^{18}O from gaseous $^{18}O_2$. After the first cycle, 89% of the oxygen of Mo═O was ^{16}O; after five cycles, 77% of the oxygen of Mo═O was still ^{16}O. The isotopic fraction of ^{16}O in the water produced upon reduction of the catalyst is very nearly equal to that of the Mo═O bonds attained in the preceding reoxidation step, suggesting that Mo═O bonds undergo complete reduction, consistent with what is shown by the Raman spectra presented in Figure 8. The small increase in the extent of ^{16}O-labeling of H_2O relative to Mo═O with increasing number of redox cycles, seen in Figure 9, is likely due to isotope exchange between the H_2O formed upon reduction and the catalyst. While this process does not contribute significantly to isotopic exchange during sequential reduction and reoxidation (see Supporting Information), it is quite important during steady-state combustion of H_2, as discussed below.

Since the oxygen leaving the cell during each reduction was primarily ^{16}O-labeled and the oxygen replenishing the reduced sample was exclusively ^{18}O-labeled, ^{18}O accumulated in the catalyst after each redox cycle. As noted earlier, one O atom per Mo atom was removed and replaced per redox cycle. Since only 11% of the molybdenyl oxygen was ^{18}O-labeled after the first redox cycle, 0.89 ^{18}O per Mo were placed into Mo−O−Si bonds and Si−O−Si bonds during the reoxidation. The amount of ^{18}O introduced into Si−O−Si bonds can be estimated from the extent of the red shift for the D_2 band. The observed shift is −0.54 cm^{-1}, which corresponds to ^{18}O substitution of 1.6% of the 18.7 exchangeable O per Mo associated with the SiO_2 surface, or 0.30 O per Mo. Thus, the majority of the 0.89 ^{18}O atoms per Mo atom retained by the catalyst after the first redox cycle are present in Mo−O−Si bonds. Sequential reduction and reoxidation leads to an increase in the fraction of ^{18}O-labeled Mo═O bonds and a decrease in the fraction of ^{16}O-labeled Mo═O bonds. This pattern suggests that during reoxidation O atoms involved in Mo−O−Si bonds are converted into Mo═O bonds.

A possible mechanism for the reoxidation of H_2-reduced MoO_x/SiO_2 by O_2 is shown in Scheme 2. O_2 is adsorbed at a four-coordinate Mo^{IV} site to yield a Mo^{VI} peroxide. The peroxide then forms a bridge with a neighboring Si atom, moving one

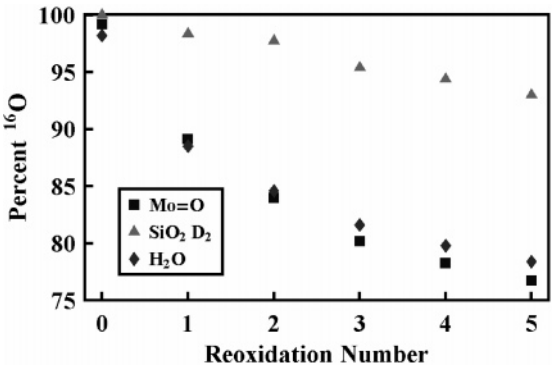

Figure 9. Isotopic composition of the Mo═O bond and the D_2 feature of SiO_2 versus the number of H_2 reduction/$^{18}O_2$ oxidation cycles performed on $^{16}O_2$-calcined MoO_x/SiO_2 at 920 K. Isotopic composition of H_2O resulting from H_2-reduction of catalyst versus number of $^{18}O_2$ reoxidations performed prior to reduction.

of the oxygens in a Mo−O−Si bond into the terminal oxo ligand of Mo═O. The unstable peroxide propagates through the SiO_2 until arriving at another Mo^{IV} center, which is then oxidized to Mo^{VI}. As drawn, the scheme does not result in ^{18}O incorporation into Mo═O bonds after a single reduction/oxidation cycle. An alternative propagation step is shown in Scheme 3, in which the peroxide formed by $^{18}O_2$ adsorption is attacked by an adjacent oxide anion rather than an adjacent siliconium cation in the first peroxide propagation step. This results in ^{18}O incorporation into one of the two Mo═O bonds after a single reduction/oxidation cycle, or 50% ^{18}O in the molybdenyl moiety. Since 11% of the molybdenyl oxygen was 18-labeled after a single cycle, it is proposed that electrophilic attack on the oxide anion occurs with 22% selectivity, and the attack on the siliconium cation with 78% selectivity. While no evidence was found for peroxide anions by Raman spectroscopy during the reoxidation of MoO_x/SiO_2, peroxide-ligated Mo complexes have been observed by Raman spectroscopy both in solution and in crystalline solids,[50,51] and are known to catalyze selective oxidation reactions in solution at low temperatures.[52] Surface peroxides have also been observed by IR spectroscopy while flowing $CH_4/H_2/O_2$ mixtures over $Fe_{0.5}Al_{0.5}PO_4$ at 623 K.[53] The inability to observe the peroxide anions during reoxidation indicates that propagation of the peroxide species occurs rapidly.

The mechanism presented in Schemes 2 and 3 leads to the incorporation of ^{18}O into the SiO_2 lattice during reoxidation of H_2-reduced MoO_x/SiO_2. The amount of ^{18}O incorporated into Si−O−Si bonds in the first step would be 0.39 O per Mo (half of 78%; the other half going into Mo−O−Si bonds), or 2.1% of the surface SiO_2 oxygen pool. This figure is consistent with the observed amount of ^{18}O incorporation after the first $^{18}O_2$ reoxidation, which was 1.6% of the surface SiO_2 oxygen pool. The average change in isotopic composition of ∼1.2% per cycle, observed over five cycles, was somewhat smaller than the change observed in the first cycle, and was due in part to the redistribution of ^{18}O to SiO_2 by H_2O formed during reduction, which is expected to exchange ∼0.65% of the SiO_2 surface oxygen per cycle based on the kinetics of $H_2{}^{18}O$ exchange (see Supporting Information). The observed changes in isotopic composition of <2.1% per cycle suggest that the average location of the SiO_2 D_2 feature on the surface is not immediately adjacent to the supported MoO_x species, so that the ^{18}O incorporation into the D_2 feature is less than the mean ^{18}O incorporation into surface Si−O−Si bonds.

Isotopic Exchange of ^{18}O and ^{16}O during Steady-State Oxidation of H_2 over MoO_x/SiO_2. H_2 oxidation by $^{18}O_2$ was studied in the same in situ Raman cell utilized to study $^{18}O/^{16}O$ exchange using $H_2{}^{18}O$. The empty Raman cell was found to be highly active for H_2 oxidation, and converted 93% of the H_2 in a 2% H_2/6% $^{18}O_2$ feed at 920 K flowing at 20 cm^3(STP)/min. H_2 conversion was ∼100% under the same flow conditions with 32.1 mg of MoO_x/SiO_2 loaded in the cell. For identical conditions (viz., feed composition, space velocity, temperature), the H_2 conversion measured in a microreactor was 20−25%. Comparisons of the dynamics of O atom exchange between

SCHEME 2: Reoxidation of H_2-Reduced MoO_x/SiO_2 by $^{18}O_2$, Resulting in No Incorporation of ^{18}O into Mo═O

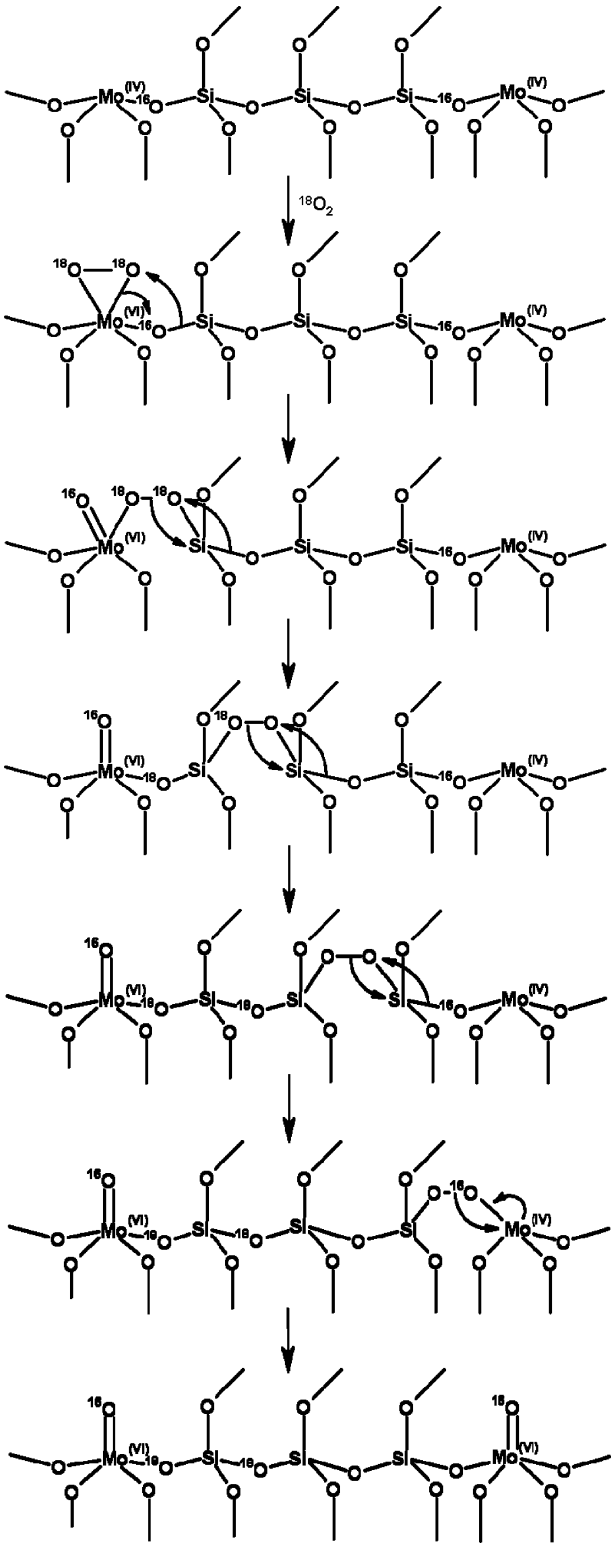

SCHEME 3: Alternative Peroxide Propagation Step Resulting in Half ^{18}O-labeled Mo═O and Half ^{16}O-labeled Mo═O

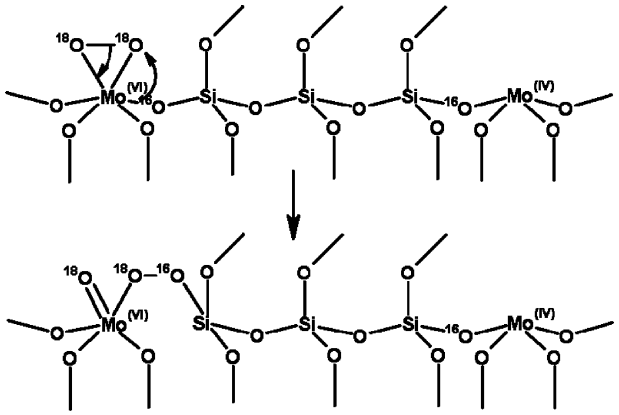

species in the gas phase and on the catalyst surface observed during the exposure of MoO_x/SiO_2 to $H_2{}^{18}O$ and to $H_2/{}^{18}O_2$ were made by analyzing results at a given value of ($p_{H_2O}t$). As noted above, the oxygen of Mo═O exchanges very rapidly with that of gaseous H_2O, so the Mo═O isotopic composition is a good indicator of the isotopic fraction of gaseous H_2O in contact with the catalyst. The data for H_2 oxidation by $^{18}O_2$ shown in Figure 10 were plotted by setting the partial pressure of H_2O at the catalyst surface to 1.2% atm (60% H_2 conversion at the catalyst position in the cell). The Mo═O trends versus ($p_{H_2O}t$) align well at all times on stream, confirming the first-order nature of the exchange reaction with respect to H_2O partial pressure and validating the approach taken to determine the H_2O partial pressure at the catalyst (see Supporting Information for details). With the partial pressure of H_2O at the surface established, the dynamics of oxygen exchange between the oxygen of the D_2 feature of SiO_2 and the gas phase during H_2 oxidation could be compared to the dynamics observed during H_2O exchange.

The trend in the isotopic composition of the oxygen of the SiO_2 D_2 feature versus ($p_{H_2O}t$) is identical during H_2 oxidation by $^{18}O_2$ over MoO_x/SiO_2 to that observed during $H_2{}^{18}O$ exchange over the same catalyst. This suggests that the incorporation of SiO_2 oxygen into the gas phase during H_2 oxidation results exclusively from exchange of surface oxygen with the H_2O produced by H_2 oxidation. If SiO_2 oxygen did participate directly in the oxidation of H_2, the kinetically limited exchange of oxygen between H_2O and the D_2 feature of SiO_2 would have been augmented by the rate of ^{16}O depletion from SiO_2 and the rate of ^{18}O incorporation into SiO_2 resulting from redox cycles, and this would have resulted in a greater apparent isotopic exchange rate for the SiO_2 D_2 feature. Such an increase in the apparent exchange rate would have been observable, since the rate of H_2 oxidation over MoO_x/SiO_2 is comparable to the rate of exchange of SiO_2 oxygen with H_2O ($\sim$3$-$5 μmol of H_2 consumed per min over MoO_x/SiO_2 versus $<$5 μmol of SiO_2 oxygen exchanged with H_2O per min). Since no enhancement in the rate of exchange was detected, the direct involvement of SiO_2 oxygen in the oxidation of H_2 can be ruled out.

The rate of oxygen exchange during reaction of $H_2/{}^{18}O_2$ was not enhanced relative to the rate of exchange with $H_2{}^{18}O$ by direct exchange of oxygen between MoO_x/SiO_2 and $^{18}O_2$. While it has been reported that direct oxygen exchange between $^{18}O_2$ and MoO_x/SiO_2 does not occur,[21] we did observe a slow exchange of O atoms between $^{18}O_2$/He and MoO_x/SiO_2. After 2 h under 10% $^{18}O_2$/He at 920 K, only about 20% of the Mo═O oxygen had exchanged, and $<$10% of the oxygen of the SiO_2

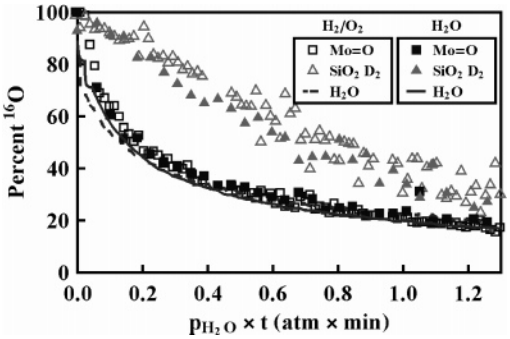

Figure 10. Comparison of temporal transients in isotopic composition of the Mo═O bond of MoO_x, the D_2 feature of SiO_2, and gaseous H_2O at 920 K during oxygen exchange between $^{16}O_2$-calcined MoO_x/SiO_2 and 3% $H_2{}^{18}O$/He, and during reaction of 2% H_2/6% $^{18}O_2$/92% He over MoO_x/SiO_2. H_2O partial pressure at the catalyst surface during H_2 oxidation was determined by aligning transients in the isotopic composition of the Mo═O bond. Total gas flow rate was 31 cm^3(STP)/min during H_2O exchange and 20 cm^3(STP)/min during H_2 oxidation. Catalyst masses were 31.5 mg during H_2O exchange and 32.1 mg during H_2 oxidation.

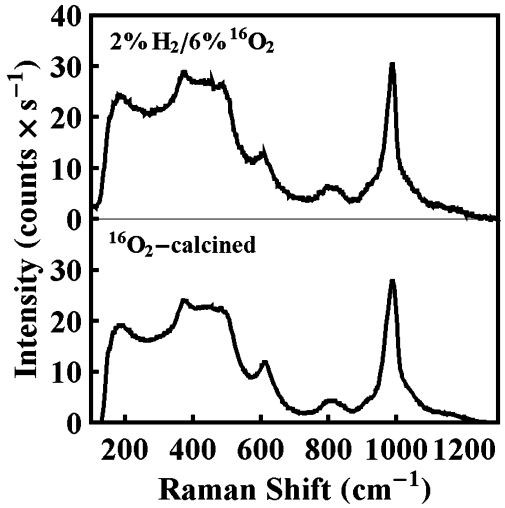

Figure 11. Baseline-subtracted Raman spectrum of MoO_x/SiO_2 acquired at 920 K in flowing 6% $^{16}O_2$/He and during reaction of 2% H_2/6% $^{16}O_2$.

D_2 feature had exchanged. More extensive exchange of oxygen occurred within only a few minutes upon exposure of MoO_x/SiO_2 to either 3.3% $H_2{}^{18}O$ or 2% H_2/6% $^{18}O_2$ at 920 K, demonstrating that the rate of direct oxygen exchange between $^{18}O_2$ and MoO_x/SiO_2 is comparatively negligible.

Figure 11 shows the Raman spectrum of MoO_x/SiO_2 during steady-state H_2 oxidation at 920 K. The spectrum is indistinguishable from that observed under flowing air at 920 K. No evidence for peroxide species was observed during steady-state H_2 oxidation, suggesting that such species react rapidly with H_2. As a consequence, the propagation of O atoms via the mechanisms shown in Schemes 2 and 3 does not occur, in agreement with the finding discussed above that ^{18}O incorporation into SiO_2 during steady-state H_2 oxidation by $^{18}O_2$ over MoO_x/SiO_2 is due exclusively to exchange between $H_2{}^{18}O$ and SiO_2. These observations suggest that the steady-state oxidation of H_2 occurs via the reaction sequence shown in Scheme 4. The rate-determining step in this mechanism is the reduction of Mo^{VI} to Mo^{IV}. Oxidation of Mo^{IV} to yield Mo^{VI} peroxide occurs rapidly, as does reduction of the peroxide to yield stable Mo^{VI} oxide to close the catalytic cycle. Consequently, only Mo^{VI}

SCHEME 4: Production and Consumption of Mo^{VI} Peroxide during Steady-State Oxidation of H_2

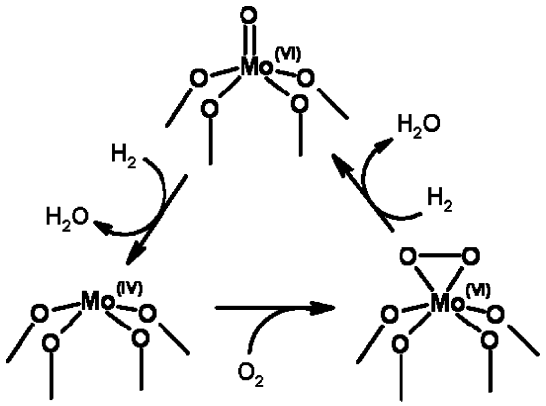

molybdate species are observed during steady-state oxidation of H_2 by O_2.

Conclusions

SiO_2-supported MoO_x is present at low loadings as isolated, pentacoordinated, mono-oxo moieties. At 920 K, the reduction of MoO_x/SiO_2 by H_2 reduces the isolated Mo^{VI} cations to Mo^{IV}. Most or all ($\geq$92%) of the H_2-reduced MoO_x is present without a terminal oxo ligand. The incorporation of 18-labeled oxygen into MoO_x and SiO_2 of MoO_x/SiO_2 can be monitored independently by quantification of the relative amplitudes of the resolved $Mo{=}^{16}O$ and $Mo{=}^{18}O$ bands, and by tracking the position of the SiO_2 D_2 feature. Direct oxygen exchange between gaseous H_2O and the surface of SiO_2 occurs with a moderate rate constant of 6.0 $(\text{atm min})^{-1}$ at 920 K. The molybdenyl oxygen of MoO_x/SiO_2 exchanges very rapidly with gaseous H_2O at the same temperature ($k > 100$ $(\text{atm} \times \text{min})^{-1}$). The presence of MoO_x on SiO_2 facilitates exchange of SiO_2 oxygen with H_2O, and about twice as much surface oxygen exchanges with a rate constant of 6.0 $(\text{atm} \times \text{min})^{-1}$ when MoO_x is present on the SiO_2 surface. During steady-state H_2 oxidation over MoO_x/SiO_2, gaseous oxygen is incorporated into both MoO_x and SiO_2. Oxygen exchange between the gas phase and SiO_2 is due exclusively to exchange with $H_2{}^{18}O$ produced by H_2 oxidation, and does not involve $^{18}O_2$ directly. Reoxidation of H_2-reduced MoO_x/SiO_2 by $^{18}O_2$ results in little ^{18}O incorporation into the oxygen of Mo=O; the majority of the ^{18}O goes into Mo−O−Si and Si−O−Si bonds. ^{18}O incorporation into the D_2 feature of SiO_2 was detected as a small but measurable red shift during the reoxidation, consistent with a proposed mechanism involving propagation of peroxide across SiO_2 during reoxidation. The peroxide propagation mechanism does not occur during steady-state H_2 oxidation, because reduction of peroxides by H_2 occurs more rapidly than the propagation of peroxides across the surface of SiO_2.

Acknowledgment. This work was supported by the Methane Conversion Cooperative sponsored by BP.

Supporting Information Available: Details regarding the quantification of oxygen pool sizes and exchange rate constants and expected change in surface composition during H_2 reduction. This material is available free of charge via the Internet at http://pubs.acs.org.

References and Notes

(1) Handzlik, J.; Ogonowski, J.; Dula, R.; Stoch, J.; Serwicka, E. M. *React. Kinet. Catal. Lett.* **2003**, *79*, 135.
(2) Jehng, J.-M.; Hu, H.; Gao, X.; Wachs, I. E. *Catal. Today* **1996,** *28*, 335.
(3) Lu, H.; Iglesia, E. *J. Catal.* **2002**, *208*, 1.
(4) Pitchai, R.; Klier, K. *Catal. Rev. Sci. Eng.* **1986**, *28*, 13.
(5) Chen, K.; Bell, A. T.; Iglesia, E. *J. Catal.* **2002**, *209*, 35.
(6) Biermann, J. J. P.; Janssen, F. J. J. G.; Ross, J. R. H. *Appl. Catal. A* **1992**, *86*, 165.
(7) Nova, I.; Lietti, L.; Casagrande, L.; Dall'Acqua, L.; Giamello, E.; Forzatti, P. *Appl. Catal. B* **1998**, *17*, 245.
(8) Mestl, G.; Srinivasan, T. K. K. *Catal. Rev. Sci. Eng.* **1998**, *40*, 451.
(9) Bañares, M. A.; Wachs, I. E. *J. Raman Spectrosc.* **2002**, *33*, 359.
(10) Ono, T.; Kamisuki, H.; Hisashi, H.; Miyata, H. *J. Catal.* **1989**, *116*, 303.
(11) Roark, R. D.; Kohler, S. D.; Ekerdt, J. G. *Catal. Lett.* **1992**, *16*, 71.
(12) Roark, R. D.; Kohler, S. D.; Ekerdt, J. G.; Kim, D. S.; Wachs, I. E. *Catal. Lett.* **1992**, *16*, 77.
(13) de Boer, M.; van Dillen, A. J.; Koningsberger, D. C.; Geus, J. W.; Vuurman, M. A.; Wachs, I. E. *Catal. Lett.* **1991**, *11*, 227.
(14) Takenaka, S.; Tanaka, T.; Funabiki, T.; Yoshida, S. *J. Phys. Chem. B* **1998**, *102*, 2960.
(15) Bañares, M. A.; Hu, H.; Wachs, I. E. *J. Catal.* **1994**, *150*, 407.
(16) Hu, H.; Wachs, I. E.; Bare, S. R. *J. Phys. Chem.* **1995**, *99*, 10897.
(17) Faraldos, M.; Bañares, M. A.; Anderson, J. A.; Hu, H.; Wachs, I. E.; Fierro, J. L. G. *J. Catal.* **1996**, *160*, 214.
(18) Bañares, M. A.; Spencer, N. D.; Jones, M. D.; Wachs, I. E. *J. Catal.* **1994,** *146*, 204.
(19) Bañares, M. A.; Hu, H.; Wachs, I. E. *J. Catal.* **1995**, *155*, 249.
(20) Desikan, A. N.; Huang, L.; Oyama, S. T. *J. Phys. Chem.* **1991**, *95*, 10050.
(21) Mauti, R.; Mims, C. A. *Catal. Lett.* **1993**, *21*, 201.
(22) Spencer, N. D. *J. Catal.* **1988**, *109*, 187.
(23) Spencer, N. D.; Pereira, C. J.; Graselli, R. K. *J. Catal.* **1990**, *126*, 546.
(24) Choi, S. H.; Wood, B. R.; Bell, A. T.; Janicke, M. T.; Ott, K. C. *J. Phys. Chem. B* **2004**, *108*, 8970.
(25) Henke, B. L.; Gullikson, E. M.; Davis, J. C. *At. Data Nucl. Data Tables* **1993**, *54*, 181.
(26) Ravel, B.; Newville, M. *Phys. Scr.* **2005**, *T115*, 1007.
(27) Su, S. C.; Carstens, J. N.; Bell, A. T. *J. Catal.* **1998**, *176*, 125.
(28) Galeener, F. L.; Mikkelsen, J. C., Jr. *Phys. Rev. B* **1981**, *23*, 5527.
(29) Galeener, F. L.; Geissberger, A. E. *Phys. Rev. B* **1983**, *27*, 6199.
(30) Uchino, T.; Tokuda, Y.; Yoko, T. *Phys. Rev. B* **1998**, *58*, 5322.
(31) Phillips, J. C. *Phys. Rev. B* **1986**, *33*, 4443.
(32) Phillips, J. C. *Phys. Rev. B* **1987**, *35*, 6409.
(33) Seyedmonir, S. R.; Abdo, S.; Howe, R. F. *J. Phys. Chem.* **1982**, *86*, 1233.
(34) Cornac, M.; Janin, A.; Lavalley, J. C. *Infrared Phys.* **1984**, *24*, 143.
(35) Cornac, M.; Janin, A.; Lavalley, J. C. *Polyhedron* **1986**, *5*, 183.
(36) Ohler, N.; Bell, A. T. *J. Catal.* **2005**, *231*, 115.
(37) Williams, C. C.; Ekerdt, J. G.; Jehng, J.-M.; Hardcastle, F. D.; Turek, A. M.; Wachs, I. E. *J. Phys. Chem.* **1991**, *95*, 8781.
(38) Iler, R. *The Chemistry of Silica*; Wiley: New York, 1979; p 635.
(39) Fournier, M.; Louis, C.; Che, M.; Chaquin, P.; Masure, D. *J. Catal.* **1989**, *119*, 400.
(40) Cramer, S. P.; Hodgson, K. O.; Gillum, W. O.; Mortenson, L. E. *J. Am. Chem. Soc.* **1978**, *100*, 3398.
(41) Wu, Z.; Xian, D. C.; Natoli, C. R.; Marcelli, A.; Paris, E.; Mottana, A. *Appl. Phys. Lett.* **2001**, *79*, 1918.
(42) Brandt, B. G.; Skapski, A. C. *Acta Chem. Scand.* **1967**, *21*, 661.
(43) Andersson, G.; Magnéli, A. *Acta Chem. Scand.* **1950**, *4*, 793.
(44) Evans, H. T., Jr. *J. Am. Chem. Soc.* **1968**, *90*, 3275.
(45) Armour, A. W.; Drew, M. G. B.; Mitchell, P. C. H. *J. Chem. Soc., Dalton Trans.* **1975**, *14*, 1493.
(46) Matsumoto, K.; Kobayashi, A.; Sasaki, Y. *Bull. Chem. Soc. Jpn.* **1975**, *48*, 1009.
(47) Busca, G. *J. Raman Spectrosc.* **2002**, *33*, 348.
(48) Ismail, H. M.; Zaki, M. I.; Bond, G. C.; Shukri, R. *Appl. Catal.* **1991**, *72*, L1.
(49) Xie, S.; Iglesia, E.; Bell, A. T. *J. Phys. Chem. B* **2001**, *105*, 5144.
(50) Arab, M.; Bougeard, D.; Aubry, J. M.; Marko, J.; Paul, J. F.; Payen, E. *J. Raman Spectrosc.* **2002**, *33*, 390.
(51) Dengel, A. C.; Griffith, W. P.; Powell, R. D.; Skapski, A. C. *J. Chem. Soc., Dalton Trans.* **1987**, 991.
(52) Maiti, S. W.; Abdul Malik, K. M.; Bhattacharyya, R. *Inorg. Chem. Commun.* **2004**, *7*, 823.
(53) Otsuka, K.; Wang, Y. *Appl. Catal. A* **2001**, *222*, 145.